From linear to nonlinear PGD-based parametric structural dynamics

Giacomo Quaranta [a], Clara Argerich Martin [b], Ruben Ibañez [c], Jean Louis Duval [a], Elias Cueto [d], Francisco Chinesta [c,*]

[a] ESI GROUP, 99, rue des Solets, 94513 Rungis cedex, France
[b] GeM, École centrale de Nantes, 1, rue de la Noe, 44321 Nantes cedex 3, France
[c] ESI GROUP Chair, ENSAM ParisTech, 151, boulevard de l'Hôpital, 75013 Paris, France
[d] Aragon Institute of Engineering Research, Universidad de Zaragoza, Edificio Betancourt, Maria de Luna, s.n., 50018 Zaragoza, Spain

A B S T R A C T

The present paper analyzes different integration schemes of solid dynamics in the frequency domain involving the so-called Proper Generalized Decomposition – PGD. The last framework assumes for the solution a parametric dependency with respect to frequency. This procedure allowed introducing other parametric dependences related to loading, geometry, and material properties. However, in these cases, affine decompositions are required for an efficient computation of separated representations. A possibility for circumventing such difficulty consists in combining modal and harmonic analysis for defining an hybrid integration scheme. Moreover, such a procedure, as proved in the present work, can be easily generalized to address nonlinear parametric dynamics, as well as to solve problems with non-symmetric stiffness matrices, always operating in the domain of low frequencies.

Keywords:
Linear and nonlinear parametric dynamics
Proper Generalized Decomposition
Harmonic analysis
Modal analysis
Low frequency domain

1. Introduction

Governing equations in solid dynamics are usually formulated either in the time or in the frequency domain. The former is preferred when calculating transient responses, whereas the frequency approach is an appealing choice for calculating forced responses. Both approaches have been extensively used and described in many classical books as, for instance, [1].

Time descriptions are used in both the linear and the nonlinear cases, being specially efficient when combined with modal analysis. The latter allows expressing the solution in a series of decoupled ordinary differential equations. Other works considered advanced space–time separated representations [2–4], for addressing transient dynamics [5–7]. Medium frequencies were efficiently attained within the Variational Theory of Complex Rays—VTCR—proposed by P. Ladeveze and intensively and successfully used (the interested reader can refer to [5] and the numerous references therein). Recently, a PGD-based dynamical integrator that takes as a parameter the field of initial conditions—conveniently expressed in a reduced basis—has also been developed [8,9].

* Corresponding author.
E-mail addresses: giacomo.quaranta@esi-group.com (G. Quaranta), clara.argerich-martin@ec-nantes.fr (C. Argerich Martin), Ruben.Ibanez-Pinillo@eleves.ec-nantes.fr (R. Ibañez), Jean-Louis.Duval@esi-group.com (J.L. Duval), ecueto@unizar.es (E. Cueto), Francisco.Chinesta@ensam.eu (F. Chinesta).

As discussed in [10–12], problems become a bit more complex in the case of parametrized dynamics, and more concretely when those parameters depend on frequency. In this case, frequency-based modeling seems more appropriate than its time counterpart, as soon as the functional forms expressing the parametric dependence on frequency is compatible with the use of a space-frequency-parameter separated representation [13–15].

We revisit in next section, for a sake of completeness, the case of linear dynamics and the harmonic-modal hybrid approach developed in [16].

2. Classical linear dynamics in the time and frequency domains

The general, semi-discretized form of the linear solid dynamics equations, writes

$$\mathbf{M}\frac{\mathrm{d}^2\mathbf{U}(t)}{\mathrm{d}t^2}+\mathbf{C}\frac{\mathrm{d}\mathbf{U}(t)}{\mathrm{d}t}+\mathbf{K}\mathbf{U}(t)=\mathbf{F}(t) \tag{1}$$

where $\mathbf{M}$, $\mathbf{C}$ and $\mathbf{K}$ are respectively the mass, damping, and stiffness matrices. Mass and stiffness matrices are usually positive definite. $\mathbf{U}$ represents the vector that contains the nodal displacements and $\mathbf{F}$ the nodal excitations (forces). The problem boundary conditions were incorporated when the space discretization leading to Eq. (1) was performed. This equation can be obtained through any suitable mesh-based discretization technique like, for instance, the Finite Element Method, and can be solved as soon as the displacements and velocities are specified at the initial time.

By moving to the frequency domain through the Fourier transform $\mathcal{F}(\bullet)$—denoting $\hat{\mathbf{F}}(\omega)=\mathcal{F}(\mathbf{F}(t))$ and $\hat{\mathbf{U}}(\omega)=\mathcal{F}(\mathbf{U}(t))$—, it results

$$\left(-\omega^2\mathbf{M}+\mathrm{i}\omega\mathbf{C}+\mathbf{K}\right)\hat{\mathbf{U}}(\omega)=\hat{\mathbf{F}}(\omega) \tag{2}$$

If damping vanishes, i.e. $\mathbf{C}=\mathbf{0}$ (if it is not the case, it is usually assumed to be proportional, $\mathbf{C}=a_0\mathbf{M}+a_1\mathbf{K}$), and one focuses on the free response of the system, $\hat{\mathbf{F}}(\omega)=\mathbf{0}$, Eq. (2) reduces to:

$$\mathbf{K}\hat{\mathbf{U}}=\omega^2\mathbf{M}\hat{\mathbf{U}} \tag{3}$$

This defines an eigenproblem whose result is given by the eigenmodes $\mathbf{P}_i$ and the associated eigenfrequencies ω_i^2. The inverse transform allows coming back to the time domain, $\mathbf{U}(t)=\mathcal{F}^{-1}(\hat{\mathbf{U}}(\omega))$.

2.1. The hybrid harmonic-modal approach

When damping is neglected, $\mathbf{C}=\mathbf{0}$ (or when proportional damping is considered $\mathbf{C}=a_0\mathbf{M}+a_1\mathbf{K}$), the single-parameter (frequency) dynamic equation reads

$$\left(-\omega^2\mathbf{M}+\mathbf{K}\right)\hat{\mathbf{U}}(\omega)=\hat{\mathbf{F}}(\omega) \tag{4}$$

We now consider matrix $\mathbf{P}$ diagonalizing matrices $\mathbf{M}$ and $\mathbf{K}$. In other words,

$$\begin{cases}\mathbf{P}^{\mathsf{T}}\mathbf{M}\mathbf{P}=\mathbb{M}\\ \mathbf{P}^{\mathsf{T}}\mathbf{K}\mathbf{P}=\mathbb{K}\end{cases}$$

where $\mathbb{M}_{ij}=m_{ii}\delta_{ij}$ and $\mathbb{K}_{ij}=k_{ii}\delta_{ij}$. Here, δ_{ij} represents the Kroenecker's delta, i.e. $\mathbb{M}$ and $\mathbb{K}$ become diagonal with entries m_{ii} and k_{ii}, respectively.

Such a choice implies that the system is no longer described in terms of its nodal degrees of freedom, but rather in terms of the modal content. Both are formally related through the linear transformation

$$\hat{\mathbf{U}}(\omega)=\mathbf{P}\boldsymbol{\xi}(\omega) \tag{5}$$

Thus, the dynamical problem reduces to [16]

$$\left(-\omega^2\mathbb{M}+\mathbb{K}\right)\boldsymbol{\xi}(\omega)=\mathbf{P}^{\mathsf{T}}\hat{\mathbf{F}}(\omega)=\hat{\mathbf{f}}(\omega) \tag{6}$$

which results in a system of N_n decoupled algebraic equations (N_n being the size of matrices $\mathbf{M}$ and $\mathbf{K}$)

$$\left(-\omega^2 m_{ii}+k_{ii}\right)\xi_i(\omega)=\hat{f}_i(\omega),\quad i=1,2,\ldots,N_n \tag{7}$$

from which it results

$$\xi_i(\omega)=\frac{\hat{f}_i(\omega)}{\left(-\omega^2 m_{ii}+k_{ii}\right)},\quad i=1,2,\ldots,N_n \tag{8}$$

that allows calculating the nodal amplitudes from Eq. (5), i.e. $\hat{\mathbf{U}}(\omega)=\mathbf{P}\boldsymbol{\xi}(\omega)$.

Thus, the space-frequency separated representation reads

$$\hat{\mathbf{U}}(\omega) = \sum_{i=1}^{N_n} \mathbf{Z}_i \, \xi_i(\omega)$$

where $\mathbf{Z}_i$ is the i-column of matrix $\mathbf{P}$.

The obtention of $\hat{\mathbf{U}}(\omega)$ allows us to come back to the time domain $\mathbf{U}(t)$ by applying an inverse Fourier transform,

$$\mathbf{U}(t) = \mathcal{F}^{-1}(\hat{\mathbf{U}}(\omega))$$

Remark. As it is usual when using harmonic analysis, the forced time response can be recovered at any time, except during the transient regime.

It is important to highlight—this will be crucial later when addressing nonlinear dynamics—that each term $\xi_i(\omega)$ involves transformed nodal forces, that is, nodal forces affected by the transformation matrix $\mathbf{P}$. Thus, Eq. (9) represents a canonical space-frequency-loading separated representation, which only makes use of a proportional damping assumption.

2.2. Extension to dynamics involving non-symmetric stiffness matrices

Above, matrices $\mathbf{M}$ and $\mathbf{K}$ were considered symmetric, making it possible to diagonalize them according to Eq. (13). Some dynamical systems, which will be discussed later, like networks composed of Helmholtz resonators, lead to non-symmetric stiffness matrices $\mathbf{K}_{\mathrm{NS}}$. The rationale considered above can be extended accordingly by just defining the symmetric matrix $\mathbf{K}_{\mathrm{S}}$ in such a way that

$$\mathbf{K}_{\mathrm{S}} = \mathbf{K}_{\mathrm{NS}} + \mathbf{K}_{\mathrm{NS}}^{\mathsf{T}} \tag{10}$$

and rewriting the dynamical system according to

$$\mathbf{M}\frac{\mathrm{d}^2\mathbf{U}(t)}{\mathrm{d}t^2} + \left(\mathbf{K}_{\mathrm{NS}} + \mathbf{K}_{\mathrm{NS}}^{\mathsf{T}} - \mathbf{K}_{\mathrm{NS}}^{\mathsf{T}}\right)\mathbf{U}(t) = \mathbf{F}(t) \tag{11}$$

or, equivalently,

$$\mathbf{M}\frac{\mathrm{d}^2\mathbf{U}(t)}{\mathrm{d}t^2} + \mathbf{K}_{\mathrm{S}}\mathbf{U}(t) = \mathbf{F}(t) + \mathbf{K}_{\mathrm{NS}}^{\mathsf{T}}\mathbf{U}(t) \tag{12}$$

Remark. The decomposition of $\mathbf{K}_{\mathrm{NS}}$ in its symmetric and skew-symmetric components can also be considered.

Thus, the left-hand side of the previous equation can be diagonalized according to

$$\begin{cases} \mathbf{P}^{\mathsf{T}}\mathbf{M}\mathbf{P} = \mathbb{M} \\ \mathbf{P}^{\mathsf{T}}\mathbf{K}_S\mathbf{P} = \mathbb{K} \end{cases} \tag{13}$$

which leads to

$$\left(-\omega^2\mathbb{M} + \mathbb{K}\right)\boldsymbol{\xi}(\omega) = \mathbf{P}^{\mathsf{T}}\hat{\mathbf{F}}(\omega) = \hat{\mathbf{f}}(\omega) \tag{14}$$

where, in the present case, $\hat{\mathbf{F}}(\omega)$ is the Fourier transform of the right-hand side of Eq. (12), i.e.

$$\hat{\mathbf{F}}(\omega) = \mathcal{F}(\mathbf{F}(t) + \mathbf{K}_{\mathrm{NS}}^{\mathsf{T}}\mathbf{U}(t)) \tag{15}$$

This term will be linearized, in the framework of an iterative scheme, by simply evaluating $\mathbf{U}(t)$ at the previous converged iteration.

The time solution can be obtained by applying the inverse transform to the frequency solution $\hat{\mathbf{U}}(\omega) = \mathbf{P}\boldsymbol{\xi}(\omega)$, according to

$$\mathbf{U}(t) = \mathcal{F}^{-1}(\hat{\mathbf{U}}(\omega)) = \mathcal{F}^{-1}(\mathbf{P}\boldsymbol{\xi}(\omega))$$

3. Nonlinear dynamics

In the nonlinear case, the general semi-discretized equilibrium equation writes

$$\mathbf{M}\frac{\mathrm{d}^2\mathbf{U}(t)}{\mathrm{d}t^2}+\mathbf{C}\frac{\mathrm{d}\mathbf{U}(t)}{\mathrm{d}t}+\mathbf{K}\mathbf{U}(t)-\mathbf{H}(\mathbf{U})=\mathbf{F}(t)$$

where the nonlinear contribution is grouped in the vector $\mathbf{H}(\mathbf{U})$ and again a proportional damping is assumed.

The simplest linearization of this equation consists in an explicit evaluation of the non-linear term $\mathbf{H}(\mathbf{U})$ at the last converged iteration. For the sake of notational simplicity, it will be denoted by $\mathbf{U}^-(t)$. Thus, as soon as the nonlinear contribution is assumed known, it can be moved to the right-hand-side member, i.e.

$$\mathbf{M}\frac{\mathrm{d}^2\mathbf{U}(t)}{\mathrm{d}t^2}+\mathbf{C}\frac{\mathrm{d}\mathbf{U}(t)}{\mathrm{d}t}+\mathbf{K}\mathbf{U}(t)=\mathbf{H}(\mathbf{U}^-(t))+\mathbf{F}(t) \tag{16}$$

An obvious possibility consists in computing the Fourier transform of the right-hand member of Eq. (16),

$$\hat{\mathbf{F}}(\omega)=\mathcal{F}(\mathbf{H}(\mathbf{U}^-(t))+\mathbf{F}(t))$$

and then to proceed exactly in the same way as in the linear case. However, in order to take benefit from model order reduction, in what follows we present an alternative but equivalent formulation, more adapted to the use of reduced bases.

By invoking the linearity of Fourier transform, we write

$$\hat{\mathbf{F}}(\omega)=\mathcal{F}\left(\mathbf{H}(\mathbf{U}^-(t))+\mathbf{F}(t)\right)=\mathcal{F}\left(\mathbf{H}(\mathbf{U}^-(t))\right)+\mathcal{F}\left(\mathbf{F}(t)\right)=\hat{\mathbf{F}}^{\mathrm{H}}(\omega)+\hat{\mathbf{F}}^{\mathrm{F}}(\omega)$$

which could be expressed using a piecewise linear approximation basis $N_l(\omega)$ (like the usually considered one in linear finite element analyses)

$$\hat{\mathbf{F}}^{\mathrm{H}}(\omega)=\sum_{l=1}^{\mathrm{L}}\hat{\mathbf{F}}^{\mathrm{H}}(\omega_l)N_l(\omega)$$

or

$$\hat{\mathbf{f}}^{\mathrm{H}}(\omega)=\mathbf{P}^{\mathsf{T}}\hat{\mathbf{F}}^{\mathrm{H}}(\omega)$$

In turn,

$$\hat{\mathbf{F}}^{\mathrm{F}}(\omega)=\sum_{l=1}^{\mathrm{L}}\hat{\mathbf{F}}^{\mathrm{F}}(\omega_l)N_l(\omega)$$

or

$$\hat{\mathbf{f}}^{\mathrm{F}}(\omega)=\mathbf{P}^{\mathsf{T}}\hat{\mathbf{F}}^{\mathrm{F}}(\omega)$$

each one contributing to the solution $\boldsymbol{\xi}(\omega)$ according to

$$\boldsymbol{\xi}(\omega)=\boldsymbol{\xi}^{\mathrm{H}}(\omega)+\boldsymbol{\xi}^{\mathrm{F}}(\omega) \tag{17}$$

with

$$\xi_i^{\mathrm{H}}(\omega)=\frac{\sum_{l=1}^{\mathrm{L}}\hat{f}_i^{\mathrm{H}}(\omega_l)N_l(\omega)}{\left(-\omega^2m_{ii}+k_{ii}\right)},\quad i=1,2,\cdots,N_n \tag{18}$$

$$\xi_i^{\mathrm{F}}(\omega)=\frac{\sum_{l=1}^{\mathrm{L}}\hat{f}_i^{\mathrm{F}}(\omega_l)N_l(\omega)}{\left(-\omega^2m_{ii}+k_{ii}\right)},\quad i=1,2,\cdots,N_n \tag{19}$$

Thus, it finally results

$$\hat{\mathbf{U}}(\omega)=\mathbf{P}\boldsymbol{\xi}(\omega)=\hat{\mathbf{U}}^{\mathrm{H}}(\omega)+\hat{\mathbf{U}}^{F}(\omega)=\mathbf{P}\boldsymbol{\xi}^{\mathrm{H}}(\omega)+\mathbf{P}\boldsymbol{\xi}^{F}(\omega)$$

being its time-dependent counterpart

$$\mathbf{U}(t)=\mathbf{U}^{\mathrm{H}}(t)+\mathbf{U}^{\mathrm{F}}(t)=\mathcal{F}^{-1}(\mathbf{P}\boldsymbol{\xi}^{\mathrm{H}}(\omega))+\mathcal{F}^{-1}(\mathbf{P}\boldsymbol{\xi}^{\mathrm{F}}(\omega))$$

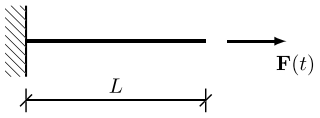

Fig. 1. Simple case study.

It is important to highlight that the inverse transform involves terms $\mathcal{T}_{il}$, $i = 1, \ldots, N_n$ and $l = 1, \ldots, \mathtt{L}$, whose form reads

$$\mathcal{T}_{il} \equiv \mathcal{F}^{-1} \quad \frac{N_l(\omega)}{-\omega^2 m_{ii} + k_{ii}}$$

that can be computed offline and stored in memory.

Our numerical experiments reveal that this offline–online procedure does not allow for significant computing time savings when one considers a standard piecewise linear approximation bases. However, by considering reduced bases to approximate functions $\hat{\mathbf{F}}^{\mathrm{H}}(\omega)$ and $\hat{\mathbf{F}}^{\mathrm{F}}(\omega)$, the number of integrals to be performed drastically reduces and the offline–online procedure becomes valuable. These reduced basis are computed offline after an adequate training stage. Moreover, the computational cost for the evaluation of the nonlinear term in the time domain $\mathbf{H}(\mathbf{U}^{-}(t))$ can be drastically reduced by using empirical interpolation techniques [17–19].

As soon as reduced bases are available in the frequency domain, their counterpart in the time domain is easily computable, and from it, direct Fourier transform could be also computed offline. The use of strategies based on the use reduced bases constitutes a work in progress.

4. Numerical results

4.1. Nonlinear dynamics

In this section, we use the proposed strategy to address the 1D dynamics of a rod of length L, cross section A, clamped at its left boundary and subjected to an axial load applied on its right boundary as depicted in Fig. 1, subjected to homogenous displacement and velocity initial conditions.

If a linear elastic behavior is assumed, the relation between the stress σ and the strain ε reads

$$\sigma = E\,\varepsilon$$

where E is the Young modulus. In every simulation, we used $L = 1$ m, $E = 2{\cdot}10^9$ N/m^2, and $\rho = 8000$ kg/m^3, where ρ is the density. When damping vanishes or when proportional damping is assumed, the mechanical response is computed from the discrete system

$$\mathbf{M}\frac{\mathrm{d}^2\mathbf{U}(t)}{\mathrm{d}t^2} + \mathbf{K}\mathbf{U}(t) = \mathbf{F}(t) \tag{20}$$

whose expression in the frequency domain is given by Eq. (4). However, when a nonlinear elastic behavior is assumed, the stress–strain relation reads

$$\sigma = \mathcal{C}(\varepsilon)$$

where $\mathcal{C}$ is a non-linear function of ε. In the numerical test here addressed, it is assumed that

$$\sigma = E\,(\varepsilon + c\,\varepsilon^3) \tag{21}$$

where c can be considered as a parameter (obviously, when $c = 0$, the nonlinear case reduces to the linear case).

Recalling the linearization described in Section 3, the mechanical response is computed from the discrete system

$$\mathbf{M}\frac{\mathrm{d}^2\mathbf{U}(t)}{\mathrm{d}t^2} + \mathbf{C}\frac{\mathrm{d}\mathbf{U}(t)}{\mathrm{d}t} + \mathbf{K}\mathbf{U}(t) = c\,\mathbf{H}(t) + \mathbf{F}(t) \tag{22}$$

where $\mathbf{H}(t)$ accounts for the nonlinear contribution.

Thus, using the notation introduced in the previous section, the frequency and time domain solutions read

$$\hat{\mathbf{U}}(\omega; c) = \hat{\mathbf{U}}^{\mathrm{F}}(\omega) + c\hat{\mathbf{U}}^{\mathrm{H}}(\omega) \tag{23}$$

that can be seen as a parametric solution involving both the frequency ω and the parameter c controlling the nonlinearity, with its time counterpart expressed from

$$\mathbf{U}(t, c) = \mathcal{F}^{-1}(\hat{\mathbf{U}}^{\mathrm{F}}(\omega)) + c\mathcal{F}^{-1}(\hat{\mathbf{U}}^{\mathrm{H}}(\omega)) \tag{24}$$

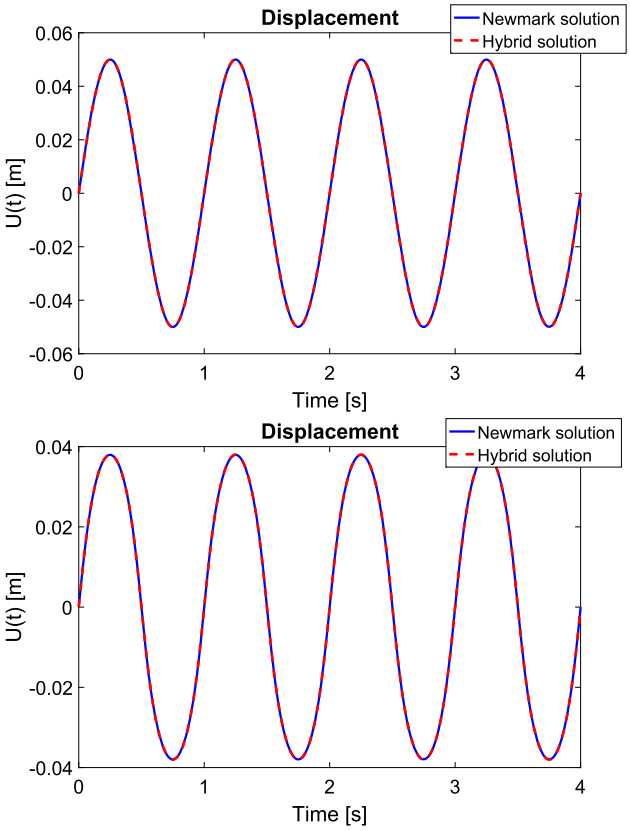

Fig. 2. Displacement at the rod right border for two different values of c: (top) $c = 0$, which corresponds to the linear case and (bottom) $c = 220$.

Table 1
Hybrid vs Newmark methods, $T = 4$ s.

	Hybrid	Newmark
$N_n = 100$	1.34 s	5.97 s
$N_n = 250$	3.26 s	14.29 s
$N_n = 500$	7.19 s	39.08 s
$N_n = 750$	11.70 s	68.12 s
$N_n = 1000$	16.33 s	100.75 s

Table 2
Hybrid vs Newmark method, $N_n = 100$.

	Hybrid	Newmark
$T = 4$ s:	1.34 s	5.97 s
$T = 8$ s:	2.44 s	12.20 s
$T = 20$ s:	6.32 s	29.75 s
$T = 40$ s:	13.54 s	59.30 s

Both formulations, the one defined in the time domain and the harmonic-modal hybrid formulations are solved in the time interval $I = [0, T]$ with $T = 4$ s, the first by using a standard Newmark time-stepping (with time step $\Delta t = 10^{-2}$ s).

Fig. 2 compares both solutions for two different values of the parameter c: $c = 0$, which corresponds to the linear case and $c = 220$ for the simple harmonic loading $F(t) = 10^{10} \sin(2\pi t)$. The computed results agree perfectly, but when using the hybrid solver, significant computing time savings are noticed. These are summarized in Tables 1 and 2. Moreover, Table 1 also reflects the fact that computing time saving remains almost independent of the considered mesh size.

Finally, we consider a more complex loading scenario, as depicted in Fig. 3. It contains a richer frequency spectrum, with $c = 0$ and $c = 4000$. The solutions when using the Newmark ($\Delta t = 10^{-3}$ s) versus the harmonic-modal hybrid schemes are again in perfect agreement, as Fig. 4 reveals, with similar computing time savings, reported in Tables 3 and 4.

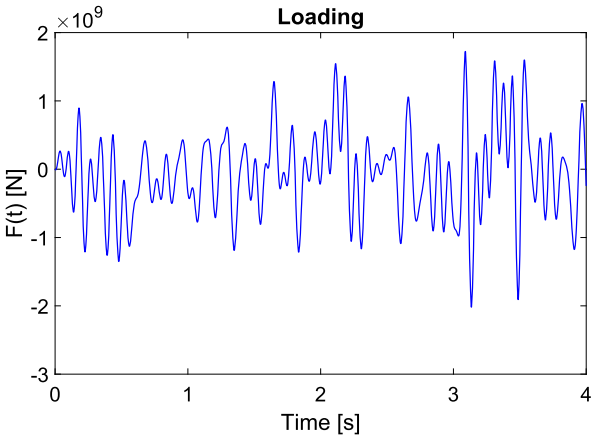

Fig. 3. *Loading containing a richer frequency spectrum.*

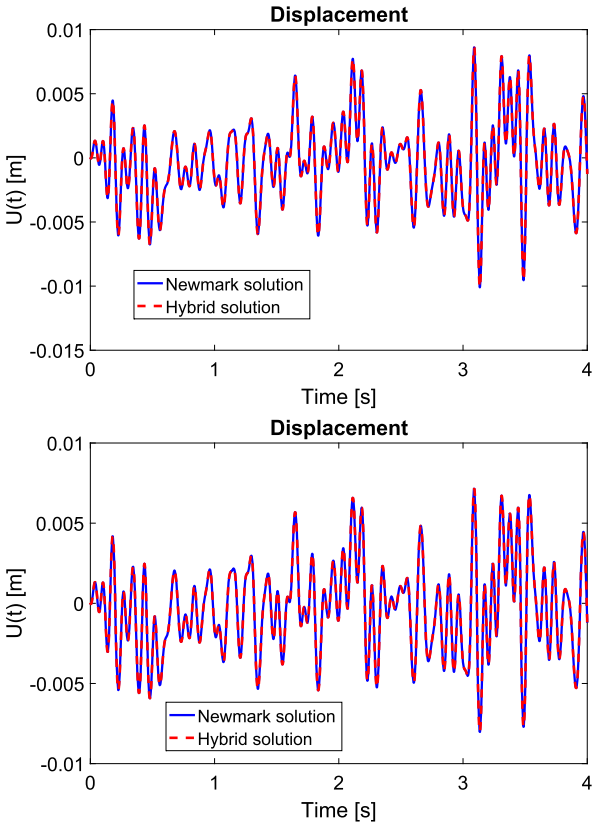

Fig. 4. Displacement at the rod right border for two different values of c: (top) $c = 0$, that corresponds to the linear case and (bottom) $c = 4000$.

Table 3
Hybrid vs Newmark method, $T = 4$ s.

	Hybrid	Newmark
$N_n = 100$:	2.49 s	9.68 s
$N_n = 250$:	6.90 s	23.38 s
$N_n = 500$:	14.28 s	48.26 s
$N_n = 750$:	21.90 s	69.72 s
$N_n = 1000$:	30.13 s	93.11 s

Table 4
Hybrid vs Newmark method, $N_x = 100$.

	Hybrid	Newmark
$T = 4$ s:	2.49 s	9.68 s
$T = 8$ s:	4.95 s	21.32 s
$T = 20$ s:	13.57 s	59.48 s
$T = 40$ s:	28.29 s	122.23 s

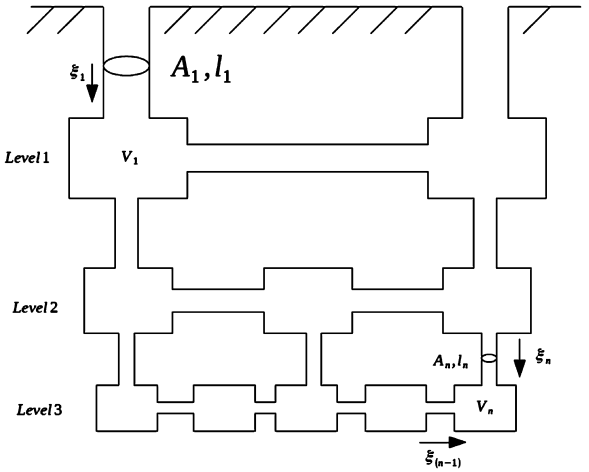

Fig. 5. Case of study for non-symmetric dynamics.

4.2. Non-symmetric stiffness

In this section, we consider a network of Helmholtz resonators, depicted in Fig. 5. Here, the oscillation amplitude of the air in each pipe contributes to the compression of the air filling the cavities connecting different tubes. That compression results in a pressure variation that generates an extra force, acting at the entrance section of each tube. In each tube, the inertia contribution involves the second time-derivative of the oscillation amplitude. The whole model results in a quite standard dynamical system with the only exception of containing a non-symmetric stiffness matrix. In that case, the modal-harmonic hybrid method is applied as described in Section 2, which proceeds by symmetrizing the problem before applying the hybrid strategy.

As can be noticed from Fig. 5, the geometry of the system follows a fractal structure. Therefore, the geometrical characteristics of subsequent generations will be determined by the characteristics of the first generation: the tube cross section, A_1, the tube length l_1, and the cavity volume, V_1. Subsequent generations are characterized by a given reduction factor, in our case of 2. Standard thermodynamical air properties are considered.

The model of a single Helmholtz resonator reads

$$\rho A L \frac{\mathrm{d}^2 U(t)}{\mathrm{d}t^2} + \frac{\gamma p A^2}{V} U(t) = f(t)$$

and, by assembling the contribution of those involved in the network of Fig. 5, it results

$$\mathbf{M} \frac{\mathrm{d}^2 \mathbf{U}(t)}{\mathrm{d}t^2} + \mathbf{K}\mathbf{U}(t) = \mathbf{F}(t)$$

where

$$\mathbf{M}_{ii} = \rho A_i L_i$$
$$\mathbf{K}_{ij} = \gamma P_0 A_i A_j \frac{1}{V^{ij}}, \text{ for } i \neq j$$

with j referring to a tube connected to one of the cavities associated with tube i, with volume V^{ij}, and

$$\mathbf{K}_{ii} = -\gamma P_0 A_i^2 \sum_{j=1}^{N_i} \frac{1}{V^{ij}}$$

where N_i refers to all the tubes connected with the cavities associated with tube i.

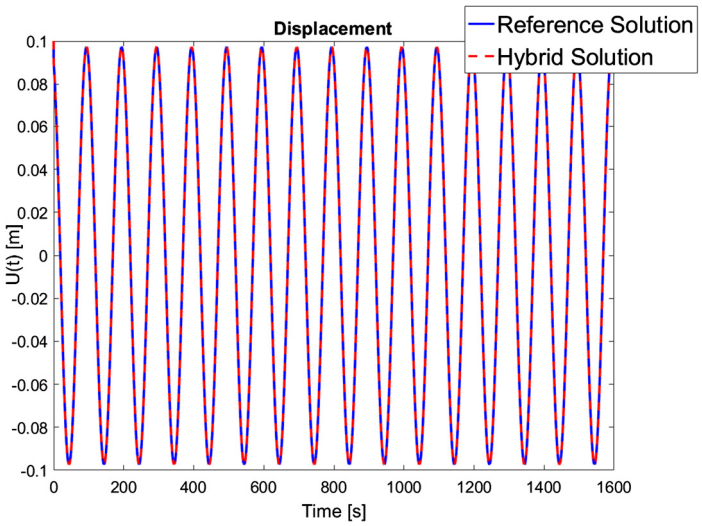

Fig. 6. Displacement of the air filling the first tube.

The discrete system involves the dynamics of the air displacement in each tube and its only specificity concerns the fact of having a non-symmetric stiffness matrix. Fig. 6 compares the solution obtained by using the modal-harmonic hybrid techniques described in Section 2 and the reference solution obtained by a standard time-stepping integration. A perfect agreement between both solutions can be noticed. The convergence is evaluated from

$$\epsilon = \frac{||\mathbf{U}^i(t) - \mathbf{U}^{i-1}(t)||}{||\mathbf{U}^i(t)||}$$

where the superscript i refers to the iteration within the hybrid strategy. The convergence is attained very fast after few iterations, three being in general enough for reducing the error by more than three orders of magnitude.

5. Conclusions

In this note, we proposed an extension of the hybrid methodology combining harmonic and modal analyses for treating nonlinear parametric dynamics.

The main contribution of the present work is the derivation of a parametric solution in the frequency space. Apart from its natural dependence on frequency, the above-developed method also accounts for other model parameters. More importantly, it explicitly decouples the dependence on the amplitude of nodal loading. This last fact makes possible the solution of nonlinear models combined with simple linearizations.

Preliminary numerical results evidence the potentialities of the proposed technique, while proving its computational efficiency.

Acknowledgements

This work has been supported by the Spanish Ministry of Economy and Competitiveness through Grants Nos. DPI2017-85139-C2-1-R and DPI2015-72365-EXP, as well as by the Regional Government of Aragon and the European Social Fund, research group T24 17R. This project has also received funding from the European Union's Horizon 2020 research and innovation programme under the Marie Sklodowska-Curie grant agreement No. 675919.

References

[1] R.W. Clough, J. Penzien, Dynamics of Structures, Civil Engineering Series, McGraw-Hill, New York, NY, 1993.
[2] P. Ladeveze, The large time increment method for the analyze of structures with nonlinear constitutive relation described by internal variables, C. R. Acad. Sci. Paris, Ser. IIb 309 (1989) 1095–1099.
[3] P. Ladeveze, Nonlinear Computational Structural Mechanics, New Approaches and Non-incremental Methods of Calculation, Springer Verlag, 1999.
[4] P. Ladeveze, L. Chamoin, On the verification of model reduction methods based on the proper generalized decomposition, Comput. Methods Appl. Mech. Eng. 200 (2011) 2032–2047.
[5] A. Barbarulo, H. Riou, L. Kovalevsky, P. Ladeveze, PGD-VTCR: a reduced order model technique to solve medium frequency broad band problems on complex acoustical systems, J. Mech. Eng. 60 (5) (2014) 307–314.
[6] L. Boucinha, A. Ammar, A. Gravouil, A. Nouy, Ideal minimal residual-based proper generalized decomposition for non-symmetric multi-field models – application to transient elastodynamics in space–time domain, Comput. Methods Appl. Mech. Eng. 273 (2014) 56–76.
[7] S. Gregory, M. Tur, E. Nadal, J.V. Aguado, F.J. Fuenmayor, F. Chinesta, Fast simulation of the pantograph-catenary dynamic interaction, Finite Elem. Anal. Des. 129 (2017) 1–13.

[8] D. Gonzalez, E. Cueto, F. Chinesta, Real-time direct integration of reduced solid dynamics equations, Int. J. Numer. Methods Eng. 99 (9) (2014) 633–653.
[9] E. Cueto, D. González, I. Alfaro, Proper Generalized Decompositions: An Introduction to Computer Implementation with Matlab, SpringerBriefs in Applied Sciences and Technology, Springer International Publishing, 2016.
[10] S.H. Crandall, The role of damping in vibration theory, J. Sound Vib. 11 (1) (1970) 3–18.
[11] C. Germoso, J.V. Aguado, A. Fraile, E. Alarcon, F. Chinesta, Efficient PGD-based dynamic calculation of non-linear soil behavior, C. R. Mecanique 344 (2016) 24–41.
[12] M.H. Malik, D. Borzacchiello, F. Chinesta, P. Diez, Inclusion of frequency dependent parameters in power transmission lines simulation using harmonic analysis and proper generalized decomposition, Int. J. Numer. Model. Electron. Netw., Devices Fields 31 (5) (2018) e2331.
[13] F. Chinesta, A. Leygue, F. Bordeu, J.V. Aguado, E. Cueto, D. Gonzalez, I. Alfaro, A. Ammar, A. Huerta, Parametric PGD based computational vademecum for efficient design, optimization and control, Arch. Comput. Methods Eng. 20 (1) (2013) 31–59.
[14] F. Chinesta, R. Keunings, A. Leygue, The Proper Generalized Decomposition for Advanced Numerical Simulations. A Primer, SpringerBriefs, Springer, 2014.
[15] J.V. Aguado, A. Huerta, F. Chinesta, E. Cueto, Real-time monitoring of thermal processes by reduced order modelling, Int. J. Numer. Methods Eng. 102 (5) (2015) 991–1017.
[16] M.H. Malik, D. Borzacchiello, J.V. Aguado, F. Chinesta, Advanced parametric space-frequency separated representations in structural dynamics: a harmonic-modal hybrid approach, C. R. Mecanique 346 (7) (2018) 590–602.
[17] M. Barrault, Y. Maday, N.C. Nguyen, A.T. Patera, An empirical interpolation method: application to efficient reduced-basis discretization of partial differential equations, C. R. Acad. Sci. Paris, Ser. I 339 (9) (2004) 667–672.
[18] S. Chaturantabut, D.C. Sorensen, Nonlinear model reduction via discrete empirical interpolation, SIAM J. Sci. Comput. 32 (5) (2010) 2737–2764.
[19] J.V. Aguado, D. Borzacchiello, C. Ghnatios, F. Lebel, R. Upadhyay, C. Binetruy, F. Chinesta, A *Simulation App* based on reduced order modeling for manufacturing optimization of composite outlet guide vanes, Adv. Model. Simul. Eng. Sci. 4 (2017) 1.